Journal of
Micro/Nanolithography,
MEMS, and MOEMS

Nanolithography.SPIEDigitalLibrary.org

Reduction in a-Si:H density utilizing a secondary plasma

Jan Uhilg
David E. Barlaz
David N. Ruzic

SPIE.

Jan Uhilg, David E. Barlaz, David N. Ruzic, "Reduction in a-Si:H density utilizing a secondary plasma," *J. Micro/Nanolith. MEMS MOEMS* **18**(4), 044502 (2019), doi: 10.1117/1.JMM.18.4.044502.

Reduction in a-Si:H density utilizing a secondary plasma

Jan Uhilg, David E. Barlaz, and David N. Ruzic*
University of Illinois at Urbana-Champaign, Center for Plasma Material Interactions, Department of Nuclear, Plasma, and Radiological Engineering, Urbana, Illinois, United States

Abstract. Following the need to improve packaging and contact layers for photovoltaics and other optoelectronic applications, a renewed interest in the fabrication of thin, low-density silicon films has arisen. We demonstrate a reactive sputtering technique utilizing a secondary plasma to crack hydrogen gas during physical vapor deposition of silicon layers. Cracking efficiency of the gas varies heavily with pressure and power from under 10% to nearly 100% conversion to hydrogen radicals. Radicals incorporated into the film produce amorphous silicon films with densities as low as 1.73 g/cm^3, compared to 2.2 g/cm^3 in their nonhydrogenated counterparts. Reduced density films likewise have a reduction in index of refraction comparable to other hydrogenated amorphous silicon produced by other techniques with indices close to 2 across the visible portion of the spectrum. Our work represents a useful, scalable advance in the production of amorphous hydrogenated silicon for a variety of applications requiring large areas. [DOI: 10.1117/1.JMM.18.4.044502]

Keywords: reactive sputtering; amorphous hydrogenated silicon; secondary plasma.

Paper 19053 received Jun. 19, 2019; accepted for publication Dec. 3, 2019; published online Dec. 28, 2019.

1 Introduction

Amorphous hydrogenated silicon (aH-Si) received extensive interest and treatment through the 1980s as a candidate material for thin film solar cell fabrication.[1] Focus on this material as a bulk absorber layer waned, as polycrystalline Si cells offered better performance and greater reductions in cost as the industry matured. In recent years, interest in aH-Si has been renewed for a variety of optoelectronic applications, including contact and buffer layers in multijunction solar cells.[2,3] The interest partially tracks an expansion in synthesis routes, but more importantly stems from the ability to alter optoelectronic response with control over hydrogen incorporation and other synthesis conditions that do not rely on silane.[4–6] Many reports of control over bandgap and refractive index are available.[7,8] Similarly, the understanding of the structure of hydrogenated amorphous films has expanded greatly from crystallinity onset and other microstructural information[5,9,10] to bond structure[11] and electronic defects.[2] Despite this, the literature is largely silent on the effect of hydrogenation on bulk density and its relation to other characteristics of interest. This paper examines how the density is changed in thin layers.

Density is expected to have a significant effect on the refractive index of a material, assuming homogeneity. The challenge is then to produce aH-Si with a reduced density, but meeting the same requirements as other layers in a thin film stack of roughness,[12] stress, etc. In order to incorporate hydrogen into the film without altering other layers, post-growth bombardment with hydrogen ions is not viable as with traditional doping methods for silicon wafers. Blister formation from energetic hydrogen has been observed when metal-hydrogen stacks are cleaned with hydrogen plasma or ion bombardment.[13,14] Incorporation of molecular hydrogen is similarly not viable as hydrogen can permeate through metals at even modest temperatures.[15] Reactive hydrogen species must, therefore, be present at the surface of the film as it grows. Options for accomplishing this during sputtering include generation of hydrogen radicals and ions by the same magnetron already in use for film deposition, an external radical source such as a remote plasma, and a secondary plasma. The first option offers no control over species production beyond changing gas composition. This can introduce a large variety of other issues as hydrogen ions will inevitably increase the current to the magnetron without an increase in deposition rate. Above some critical flux, this resistive heating could cause problems for brittle silicon deposition sources, as well as significant chemical etching of the source. External radical sources are attractive if they can be entirely independently controlled, but this would likely require a differential pumping system of some kind. Additionally, there would be significant challenges to the scalability of such a technique as the beam would need to be uniform over the area of increasingly large solar cell arrays and other panel size devices. A secondary plasma may be the most attractive option as physical vapor deposition (PVD) chambers will already be running at low pressures (few mTorr) so an radio-frequency (RF) generated inductively or capacitively coupled plasma will have reasonable uniformity over the areas required. Secondary plasmas generated by RF power have already been demonstrated and do not have a significant impact on magnetron performance or stability[16] required for consistent deposition rates. The greater concern will be whether the use of RF power will cause the substrate to overheat inducing undesired crystallization.[17]

In the past, hydrogenated silicon films have been observed to be amorphous, exhibiting some short-range order with densities as low as 1.55 g/cm^3 as opposed to 2.32 g/cm^3 for crystalline Si[9]. Previous attempts to incorporate such material into a stacked structure has led to the growth of blisters,[14] worm like structures,[18] and other surface roughening[19] features that will counter any performance gains from reduced density. The goal of this work is to test

*Address all correspondence to David N. Ruzic, E-mail: druzic@illinois.edu

1932-5150/2019/$28.00 © 2019 SPIE

the efficacy of a secondary plasma in producing amorphous silicon films of reduced density for solar cell contact layers and other opto-electronic devices. The expectation is that there exists a parameter space, in which atomic hydrogen may be incorporated into the film lowering density without the formation of blisters.

2 Experimental Setup/Methodology

Samples were grown using a side-by-side, dual magnetron PVD chamber, with an imbalanced magnetic field configuration. Both magnetrons are 10.16 cm diameter Kurt J Lesker TORUS, with them having inverse polarity magnetic field configurations with respect to one another and were fitted with Mo and Si targets (Lesker, >99.9999%). Both were operated using a direct current (DC) bias with either a MagnaPower XR Series 2 kV, 1 A or a Bertan Series 105, 2 kV, 0.5 A power supply. A pneumatically operated shutter was in place that could be moved to cover one of the magnetrons preventing deposition on the sample without turning the magnetron off. The shutter was found to effectively prevent cross contamination of the sputter targets by x-ray photo-electron spectroscopy (XPS) surveys of the targets after removal.

The secondary plasma was generated using an in-house made coil made from 1 cm copper tubing (McMaster-Carr) cut to form a three-loop coil extending from an RF insulated two-tube feedthrough. Connections on the vacuum side were made with Swagelok tube compression fittings, and on the outside the tube feedthrough was fit to Swagelok tube "T" with one port connected to cooling water and the last connected to a coaxial cable from the matching network. The coil was conformally hand wrapped with fiberglass tape followed by Kapton tape on sections where the highest point to point voltage differences on the coil were expected to prevent shorts and arcs. The RF power was produced with a Kurt J Lesker R-series RF power supply and fed through an in-house made matching network in an "L" configuration with variable capacitors (64 to 232 pF shunt and 22 to 61 pF parallel) and a variable inductor (0 to 17 μH).

The chamber was consistently pumped to base pressures below 5×10^{-7} Torr. Argon and hydrogen (Airgas, 99.9999%) were regulated via mass flow controllers. Hydrogen was fed through a T in the line with two pneumatically controlled lift valves, one to the chamber and the other to an exhaust pump. The lift valves and magnetron shutter were actuated by solenoid valves regulating a compressed air source, the solenoids were controlled by a custom Labview program capable of programming shutter control and hydrogen entry independently. This allowed the introduction of hydrogen to be delayed until after silicon deposition had begun, as well as turned off before deposition was completed. Cleaning plasmas were run in argon for up to 30 min before samples were grown to remove oxides from sputter targets to ensure uniformity of deposition rates between samples (Fig. 1).

Samples were grown on 2.54 cm coupons cleaved from silicon wafers (MEMS Engineering and Material, undoped) in a clean hood and cleaned with isopropanol before being dried with filtered compressed nitrogen gas (Airgas, 99.9999%). All silicon thin films were deposited on ~2 nm of Mo to ensure contrast when probed with x-rays.

Film thickness, density, and roughness were determined by grazing incidence x-ray reflectivity (XRR) on a panalytical x-ray difractometer. The copper x-ray source operated at 45 kV and 40 mA. The detector was a pixel high-speed line detector capable of 25 million counts per second per strip. A 1/32-deg divergence slit was used on the beam optics. Data modeling was performed using IMD software[20] based on XRR theory.[21] Film thicknesses were confirmed using step height measurements with a Dektak 3030 stylus profilometer.

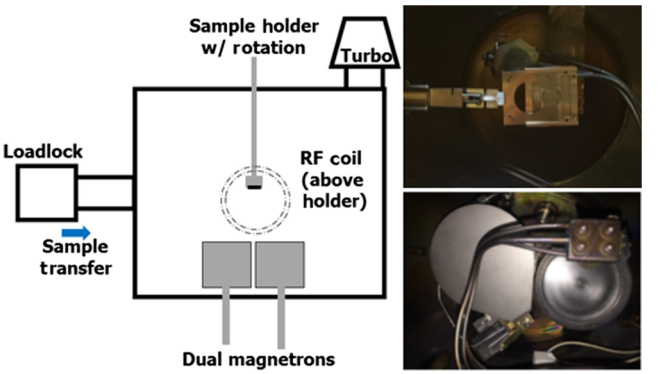

Fig. 1 Schematic (left) of the dual magnetron chamber used. RF coil is ~6 in. above the center line of the sample holder and magnetrons. Dual magnetrons with shutter shown bottom right, sample holder, and transfer arm shown top right. A quartz crystal microbalance can be seen in both images. Magnetron throw distance is ~70 mm.

An Asylum Research MFP-3D™ atomic force microscopy (AFM) tool was used for AFM measurements. Tips were budget sensors BS-Tap300Al tapping tips with a lateral resolution of ~8 nm when new. All measurements were performed in tapping mode. Image processing, surface roughness measurements, and other analyses were performed using the Igor Pro software package used to control the AFM.

Hydrogen radical concentrations were acquired using in-house built radical probes. The probes employ a series of thermocouples (Omega, KMQXL-062U-12) half of which are reference (uncoated, stainless steel sheath), and half of which are Au coated by electroplating (Fig. 2). The Au coating acts as a catalytic recombination site for hydrogen radicals, which provide differential heating of the probe in addition to energy from other plasma species and microwave heating present on both probes. For an extended discussion on the theory, design, and function of the probes, see Refs. 22 and 23.

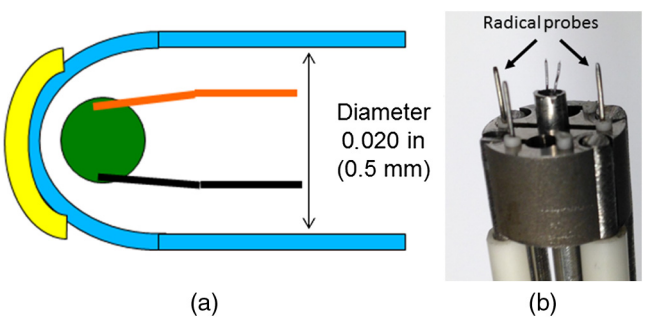

Fig. 2 (a) Schematic (not to scale) of radical probe tip. Au coating (yellow) is 1 to 5 μm in thickness. (b) Completed probe assembly shown with three radical probes.

3 Results

3.1 *Mo Contrast Layer*

Si thin films grown on Si substrates are difficult to characterize without a layer of significantly different density in between. For that reason, thin films of Mo were grown to calibrate the growth rate as a function of magnetron power and to confirm that films produced were both conformal and uniform in thickness and density. Sputtering was performed in 1.5 mTorr of Ar with a current setpoint of 0.25 A producing a nominal bias of 320 V. Films were grown to ∼50 nm for ease of XRR data acquisition. Reproducible deposition rates of 10.5 nm/min were consistently observed as long as cleaning plasma protocols were followed. Films densities were consistently $9.8 \pm 0.5\%$ g/cm^3. As shown in Fig. 3, the model built for the film requires the modeling of a ∼1-nm MoO_3 film in order to accurately predict film roughness. Mo, like most metals, does not grow a self-limiting oxide. When XRR of films was delayed more than ∼6 h, the modeled MoO_3 thickness was above ∼1 nm. Surface roughness of the Mo films was below 0.25 nm, less than one atomic layer, (see Fig. 3 inset) indicating that the Mo films were of uniformity required to determine roughness of the subsequent silicon layer accurately.

3.2 *Amorphous Si*

To produce a-Si films, both magnetrons were struck simultaneously in 1.5 mTorr of Ar with the shutter covering the Si magnetron. The Mo deposition was run for 5 to 6 s to produce a contrast layer of 2 to 3 nm on the wafer coupon. The Si deposition was started by flipping the shutter position to cover the Mo magnetron. Both magnetrons would be kept on during Si deposition to ensure no Si contamination of the Mo magnetron. *Ex situ* XPS of the Si films confirmed that no Mo contamination was present within XPS detection limits.

The Si magnetron was operated with a current setpoint of 50 mA and a nominal bias after cleaning plasma of 750 V. As with the Mo films, Si films were grown thicker than the ultimate ∼10 nm needed for optoelectronics manufacturing for ease of analysis. Films around 20 nm were consistently produced with a density of 2.2 (error bars) g/cm^3 at a deposition rate of 3.6 nm/min. Si is known to grow a self-limiting oxide of ∼2 nm at room temperature and oxide layers were frequently used to assist in modeling of Si films characterized by XRR. The fit shows in Fig. 4 similarly as a MoO_3 layer built into the model as part of the contrast layer below the Si film. AFM micrographs displayed a surface roughness higher than that of the Mo films, however, the roughness was consistently no more than 10% of the film thickness as seen in Fig. 5. It is reasonable to assume that as film thickness is reduced to length scales appropriate for solar cell contact and buffer layers that this surface roughness would reduce accordingly and not be of concern.

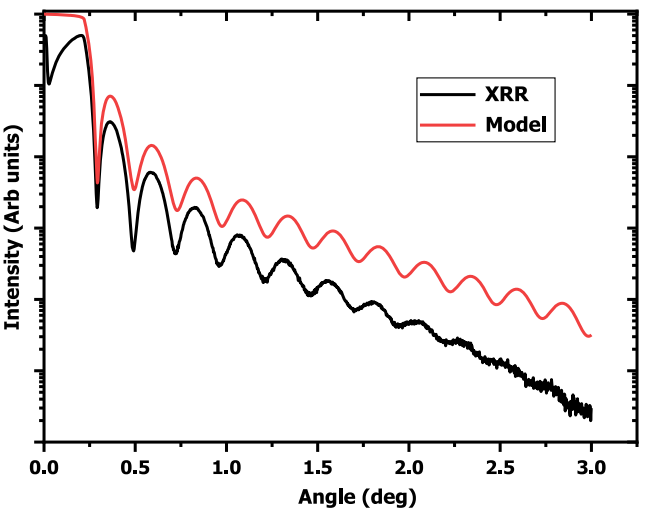

Fig. 4 XRR data and model for a 17-nm Si film with a density of 2.2 g/cm^3.

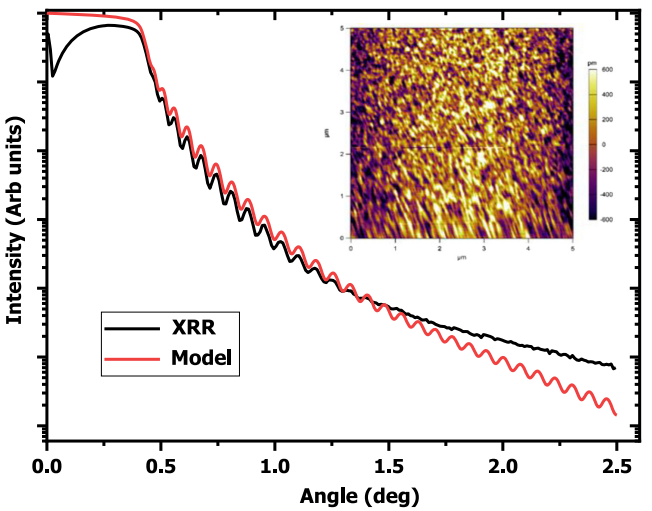

Fig. 3 XRR data and fit for a 53-nm Mo film (roughness < 1 nm) with a 1-nm MoO_3 oxide cap. Inset is 5×5 μm AFM micrograph (color scale bar ±600 pm). Streaking at the bottom 5% of the image was due to variance in the tip drive amplitude and may be disregarded when determining film roughness.

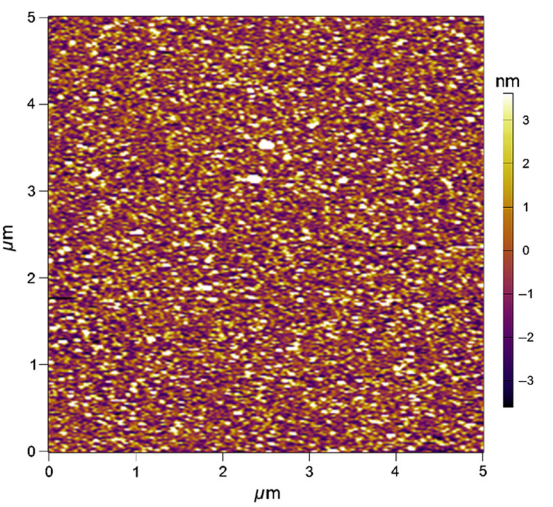

Fig. 5 AFM micrograph of a 20-nm amorphous Si film with a surface roughness of 2 to 3 nm. The two bright white spots slightly above center in the image are both nanoparticles almost identical at 40 nm in diameter. They are most likely contamination particles produced by the magnetron target erosion.

3.3 *Hydrogenated Amorphous Silicon*

Before hydrogenated silicon could be produced, the effect of hydrogen on the Mo contrast was determined to ensure sufficient contrast remained between the hydrogenated silicon film and the wafer. Mo films were grown to similar thicknesses as before with varying concentrations of hydrogen present. Mo density decreased by ~ 1 g/cm^3 without significant changes to surface roughness. To ensure that the contrast layer was unchanged, the shutter and lift valve program was set to delay the introduction of hydrogen into the chamber until several seconds after Si deposition began. A similar delay was programmed to end the hydrogen flow several seconds before the deposition was set to end. This was partially to mimic the "capping layer" of nonhydrogenated silicon seen in similar work,[19] as well as to ensure no hydrogen would be present in the chamber when deposition of a subsequent layer began in a final solar cell stack.

In order to search for the parameter space within which silicon films of reduced density may be produced without blistering, sweeps were made across a variety of process conditions. Hydrogen pressure was varied from 0.1 to 6 mTorr and RF power was varied up to 300 W forward power. Hydrogen ions (primarily H_2^+) are generated by both the magnetron plasma and RF coil to a comparable degree as argon ions, necessitating a recalibration of the setpoints and deposition rates. TRIM/SRIM models were run to predict any changes in sputtering yield. At the biases used, the contributions to target erosion of both Mo and Si were negligible. Contributions of SiH_4 production from the target or deposited film were ignored as they should be slow relative to growth rates. Likewise, contributions from scattering were discounted as operating pressures were never going to exceed 7.5 mTorr total (collisionless regime for a 70-mm throw distance) and the ability of H_2 gas molecules to scatter much heavier Si and Mo atoms is limited.

Hydrogen radical concentrations were measured for a variety of RF powers starting at the lowest pressure possible with the flow rate range of the MFC. It was quickly observed that the generation of hydrogen radicals (beyond what the magnetron plasma generates) is a weak function of both RF power and H_2 partial pressure. Indeed, Fig. 6 shows increases in radicals with power barely above the uncertainty level shown by the error bars. In the case of pressure, changes to radical density are within the error of the measurement, but appear to show a decrease in concentration with pressure that may be explained by a decrease in the cracking efficiency of the plasma as the number of hydrogen bonds present increases. Results were confirmed by repeating scans (not shown) with measured radical concentrations decreasing several percent than initially measured as is expected due to degradation in the catalytic surface of the probe.

Based on calculated densities for the pressures used, molecular hydrogen should be delivered before plasma ignition at a concentration of 1×10^{13} molecules/cm^3. Full conversion of molecular hydrogen to radicals (with no ionization) would be double the molecular concentrations. With the radical concentrations measured, this would produce radical production efficiencies of $\sim 10\%$ for low power and high pressure, and approaching 100% for lower pressures. Confirmation of radical production efficiency would require higher precision measurements of ion densities and subsequent correction for argon ions.

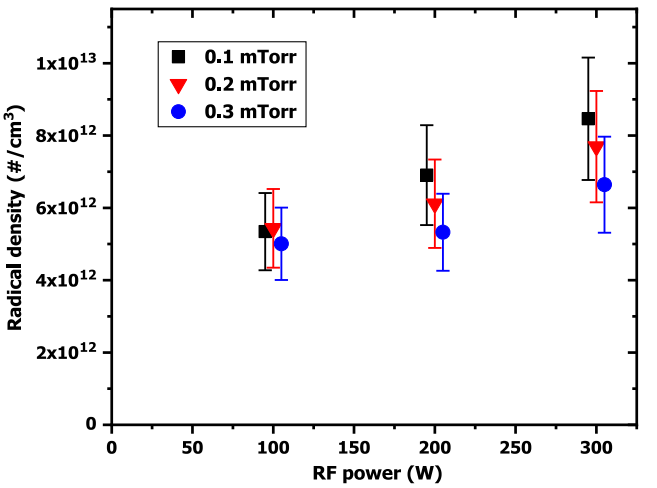

Fig. 6 Hydrogen radical concentrations measured by radical probes at varying pressures and RF powers. Offsets added to data in *x* axis for ease of viewing. Error bars are 20% of measured values based on error propagation from thermocouple accuracy and uncertainty in measured recombination coefficient for H radicals on Au.

Lacking high-precision measurements or estimations of ion densities, changes to the Si magnetron setpoints were altered heuristically. To achieve comparable deposition rates as before hydrogen was introduced, the current setpoint on the magnetron was increased to 100 mA when hydrogen gas was present without the secondary plasma. The setpoint was further increased to 150 to 200 mA when the RF coil was in use.

Early samples at higher hydrogen pressures ($\sim$5 mTorr) without a secondary plasma exhibited XRR behavior indicative of an exceptionally rough film. An example of this is shown in Fig. 7 as the close packed fringes of the main Si film are not visible over about half of the scan range, and the intensity drops off about twice as fast as expected. Fitting the spacing of the film fringes offered a density of 1.2 g/cm^3, significantly lower than was expected to be achievable by this route. SEM (Fig. 8) and AFM micrographs confirmed not only that the blisters were present, but

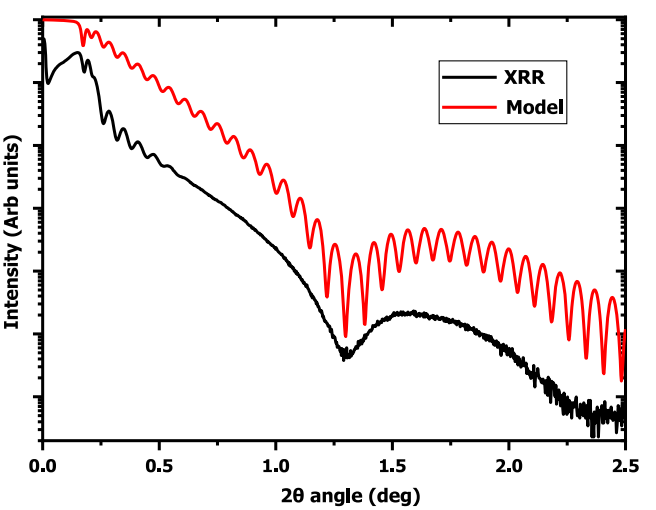

Fig. 7 XRR data and fit of a hydrogenated silicon film with a loss of fringe visibility from blister induced roughness.

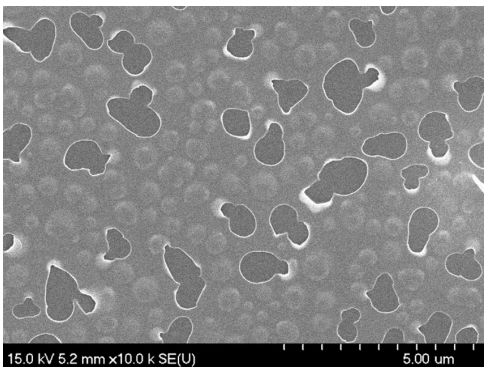

Fig. 8 SEM micrograph of a 60-nm silicon film deposited with a 5-mTorr partial pressure of H_2.

the stress induced by the blisters caused delamination of the film in places. The largest blisters were raised nearly 100 nm, significantly >60 nm overall thickness of the film.

Similar results appeared at this pressure with the RF coil in use suggesting both a limitation to the possible uptake rate of hydrogen by the growing film, as well as the possibility of "boiling" the hydrogen out of the film by the RF coil due to the increased temperature of the sample during deposition. At 300 W, substrate temperatures as high as 120°C were observed. Modifications were made to mitigate this including surrounding the sample with copper tape to improve thermal conductivity to the mount as well installing a "heat shield" made from stainless steel shim stock between the sample and the coil. The assumption was that the sample mount, being grounded to the chamber, was one of the closest ground planes where current from the coil left the plasma. The only ground plane closer to the coil was the top of the chamber body directly above the coil. The heat shield would provide a additional ground plans closer to the sample and remove line of sight from the sample to the coil. Radicals created in the throw path of the magnetrons would still have unimpeded access to the sample.

The design of experiment that followed focused on the pressures used in the radical probe scans. Efforts to further increase the RF power were not possible due to overheating of the RF feedthrough. The results of this experiment are summarized in Table 1.

The trend suggested by Fig. 6 is supported here as increases in RF power produce a greater effect than increasing the hydrogen partial pressure. In other words, driving 300 W into the secondary plasma produces a film of lower density than any film grown at higher pressure and lower

Table 1 Densities of amorphous hydrogenated silicon films at varying H_2 partial pressures and RF powers. Errors maybe estimated as 2% of the reported values based on software limitations.

		H_2 pressure (mTorr)		
Density (g/cm^3)		0.1	0.2	0.3
RF power (W)	100	2.1	N/A	1.91
	200	N/A	N/A	1.96
	300	1.89	1.83	1.73

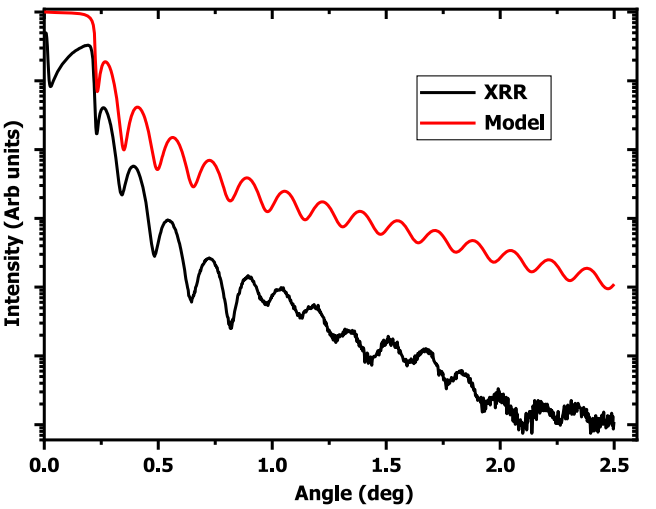

Fig. 9 XRR plot and model for a 26-nm hydrogenated silicon film with a measured density of 1.73 g/cm^3 deposited with a H_2 partial pressure of 0.3 mTorr and a secondary plasma power of 300 W.

power. XRR models consistently produced close fits to the slope of the data near the critical angle regardless of intensity loss. The experimental data and fit of the 300 W, 0.3 mTorr sample are shown in Fig. 9. Unfortunately, this sample also appeared to have blisters present as seen in the AFM micrograph displayed in Fig. 10.

Reducing the hydrogen partial pressure to 0.1 mTorr, while giving a higher aSi:H density (1.89 versus 1.73 g/cm^3), produced a film with many fewer bubbles. Figure 11 shows an AFM with a reduced bubble count.

To determine the effect of reduced density, spectroscopic ellipsometry was performed on select samples using a Woollam VASE ellipsometer scanning across the visible and near IR region at angles of incidence ranging from 50 deg to 70 deg. Film stacks were modeled by two methods to check for consistency, both using the Woollam software's Cody–Lorentz model for Palik's amorphous Si data (Ref. 24, Table XIV). One model treated the film as a single layer of unknown density but no void space in the film, a second model treated the film as an effective medium approximation

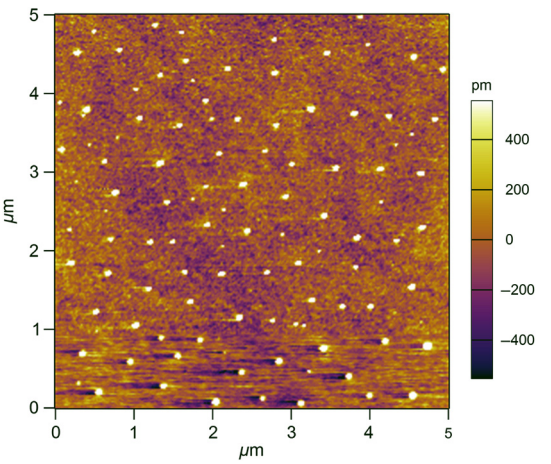

Fig. 10 AFM micrograph of a 26-nm hydrogenated silicon film with a measured density of 1.73 g/cm^3 deposited with a H_2 partial pressure of 0.3 mTorr and a secondary plasma power of 300 W.

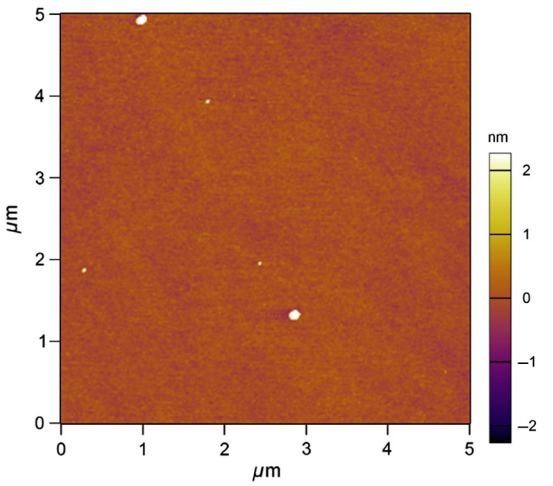

Fig. 11 AFM of a 25-nm hydrogenated Si sample grown with a hydrogen partial pressure of 0.1 mTorr and 300 W of secondary plasma. Resulting density was 1.89 g/cm^3 with an RMS roughness of 125 picometers excluding bubbles.

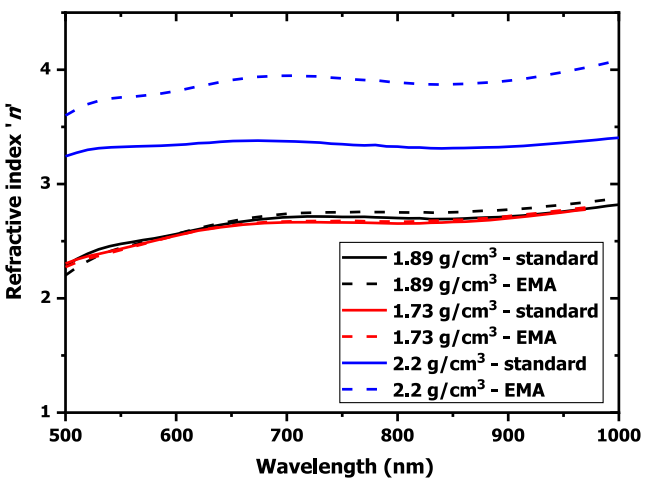

Fig. 12 Refractive index (n) as a function of wavelength for two hydrogenated silicon films (black + red) and a nonhydrogenated silicon reference (blue). Dashed lines refer to the EMA model with voids.

(EMA) layer of silicon and void space. In both cases, the total thickness was known from XRR, but the optical constants were fit by the software along with the void fraction in the EMA model. The extracted optical constants are shown in Fig. 12. Values for the extinction coefficient k (not shown) were consistently below unity as expected for such materials.

4 Discussion

As anticipated the greatest roadblock to reduce the density of silicon was the formation of blisters when the Si film is grown in the presence of hydrogen. The use of a secondary plasma offers a potential solution in that it is able to increase the concentration of radicals available at the free surface of a growing film without significantly raising the deposition pressure. Although higher powers may be able to generate marginally more radicals at the same total pressure, the most important experimental parameter for suppressing hydrogen blister formation is hydrogen partial pressure.

As evidenced by Fig. 10, full prevention of blisters from hydrogenation has not yet been achieved in the lowest density thick aSi-H films. Figure 11 shows that if a moderately higher density is acceptable, such films without visible blisters are possible. Note that these AFM and micrographs are for ~30-nm thick films. When that thickness decreases to the length scales desired for certain optoelectronic applications, it may be impossible for a blister to form at all. Demonstrated improvements offer an expectation that future work will manage to remove such blisters entirely even in a thick film. In the previous work discussed, efforts to hydrogenate silicon without the use of a secondary plasma caused the formation of blisters and larger worm like structures. Such features were reproduced here at hydrogen partial pressures in the single digits of mTorr and were largely removed.

The use of a secondary plasma was able to produce significantly reduced density films at much lower hydrogen partial pressures by increasing radical production as opposed to incorporating molecular hydrogen. The result is that the blisters have shrunk in size down to 5 nm for a 20-nm film. This blister size will not necessarily follow linearly with film thickness. One might imagine that if the blisters are ~25% of film thickness for the conditions shown, a 10-nm Si film in a multilayer solar cell stack would have a blister roughness of 2 nm without the potential for large-scale delamination. It is possible that for a thin film of such a small length scale that blisters would fail to form entirely. The authors expect to reduce the size and distribution of these blisters with the addition of active cooling to the sample mount, and better prevention of radiative heat flux from the RF coil during deposition, and the possible addition of more RF power. As expected, the index of refraction is a strong function of film density, and the indices measured were significantly less than those observed in Fig. 3 of Ref. 7.

5 Conclusions

A secondary plasma was successfully used to improve the generation of hydrogen radicals for incorporation into an amorphous hydrogenated silicon thin film grown by DC sputtering. The resultant films possessed densities as low at 1.73 g/cm^3. Blister formation is reduced to a roughness of <25% of film thickness as compared to hydrogenated silicon grown without a secondary plasma and without any evidence of delamination.

Acknowledgments

Sample characterization was carried out in part in the Frederick Seitz Materials Research Laboratory Central Research Facilities, University of Illinois. We wish to thank Dr. Mauro Sardela and Dr. Julio Soares for assistance with fitting XRR and Ellipsometry data, respectively.

References

1. W. Paul and D. A. Anderson, "Properties of amorphous hydrogenated silicon, with special emphasis on preparation by sputtering," *Solar Energy Mater.* **5**(3), 229–316 (1981).
2. M. Stuckelberger et al., "Review: progress in solar cells from hydrogenated amorphous silicon," *Renew. Sustainable Energy Rev.* **76**, 1497–1523 (2017).
3. J. Fang et al., "High-quality hydrogenated intrinsic amorphous silicon oxide layers treated by H_2 plasma used as the p/i buffer layers in hydrogenated amorphous silicon solar cells," *Solar Energy Mater. Solar Cells* **136**, 172–176 (2015).

4. X. Zhang et al., "Sputtered hydrogenated amorphous silicon for silicon heterojunction solar cell fabrication," *Energy Procedia* **55**, 865–872 (2014).
5. A. M. Myers et al., "Monte Carlo simulations of magnetron sputtering particle transport," *J. Vac. Sci. Technol. A* **9**(3), 614–618 (1991).
6. K. Xu et al., "Micro optical sensors based on avalanching silicon light-emitting devices monolithically integrated on chips," *Opt. Mater. Express* **9**(10), 3985–3997 (2019).
7. D. Gibson et al., "Optical properties of sputter deposited amorphous hydrogenated silicon films," in *Opt. Interference Coat.*, Optical Society of America, ThC.2 (2016).
8. Y. Shiratori et al., "Effect of RF power on the properties of intrinsic hydrogenated amorphous silicon passivation layer deposited by facing target sputtering," *Appl. Phys. Express* **11**(3), 031301 (2018).
9. A. G. Revesz, "On the structure of noncrystalline Si and $Si_{1-x}H_x$ films," *Phys. Status Solidi A* **60**(2), 619–629 (1980).
10. J. A. Peck et al., "High deposition rate nanocrystalline and amorphous silicon thin film production via surface wave plasma source," *Surf. Coat. Technol.* **325**, 370–376 (2017).
11. A. H. M. Smets et al., "The relation between the bandgap and the anisotropic nature of hydrogenated amorphous silicon," *IEEE J. Photovoltaics* **2**(2), 94–98 (2012).
12. P. Photopoulos and A. G. Nassiopoulou, "Room- and low-temperature voltage tunable electroluminescence from a single layer of silicon quantum dots in between two thin SiO_2 layers," *Appl. Phys. Lett.* **77**(12), 1816–1818 (2000).
13. A. S. Kuznetsov, M. A. Gleeson, and F. Bijkerk, "Temperature dependencies of hydrogen-induced blistering of thin film multilayers," *J. Appl. Phys.* **115**(17), 173510 (2014).
14. D. T. Elg et al., "In situ collector cleaning and extreme ultraviolet reflectivity restoration by hydrogen plasma for extreme ultraviolet sources," *J. Vac. Sci. Technol. A* **34**(2), 021305 (2016).
15. T. Tanabe, Y. Yamanishi, and S. Imoto, "Hydrogen permeation and diffusion in molybdenum," *J. Nucl. Mater.* **191–194**, 439–443 (1992).
16. R. Raju et al., "Development and characterization of a secondary RF plasma-assisted closed-field dual magnetron sputtering system for optical coatings on large-area substrates," *Plasma Sources Sci. Technol.* **19**(2), 025011), (2010).
17. R. W. Collins et al., "Evolution of microstructure and phase in amorphous, protocrystalline, and microcrystalline silicon studied by real time spectroscopic ellipsometry," *Solar Energy Mater. Solar Cells* **78**(1), 143–180 (2003).
18. A. J. Flewitt et al., "In-situ scanning tunnelling microscopy of hydrogenated amorphous silicon andmicrocrystalline silicon," *Appl. Phys. A* **66**(Suppl 1), 1101–1105 (1998).
19. M. J. H. Kessels et al., "Si adhesion interlayer effects in hydrogen passivated Si/W soft x-ray multilayer mirrors," *Surf. Sci.* **600**(6), 1405–1408 (2006).
20. D. L. Windt, "IMD—software for modeling the optical properties of multilayer films," *Comput. Phys.* **12**(4), 360–370 (1998).
21. I. Kojima and B. Li, "Structural characterization of thin films by x-ray reflectivity," *Rigaku J.* **16**(2), 31–42 (1999).
22. M. Mozetič et al., "Determination of density of hydrogen atoms in the ground state," *Vacuum* **47**(6), 943–945 (1996).
23. D. T. Elg et al., "Modeling and measurement of hydrogen radical densities of *in situ* plasma-based Sn cleaning source," *J. Micro/Nanolithogr. MEMS MOEMS* **16**(2), 023501 (2017).
24. E. D. Palik, *Handbookof Optical Constants of Solids.* Academic Press, San Diego, California (1985).

Biographies of the authors are not available.